Journal of Physics: Conference Series **2930** (2024) 012004 doi:10.1088/1742-6596/2930/1/012004

Radiofrequency Coil Tuning Using Matching Circuit Co-Simulation with Magnetic Resonance Integral Equations

Amer Ajanovic[1,2,3*], Stephen Ogier[3], Raphael Tomi-Tricot[3,4], Joseph V Hajnal[3,5,6], Shaihan J Malik[3,6]

[1] Faculty of Science, University of Sarajevo, Sarajevo, Bosnia and Herzegovina
[2] Accelerator Beam Physics Department, CERN, Geneva, Switzerland
[3] Biomedical Engineering Department, King's College London, London, UK
[4] MR Research Collaborations, Siemens Healthcare Limited, Surrey, UK
[5] Centre for the Developing Brain, School of Biomedical Engineering and Imaging Sciences, King's College London, London, UK
[6] London Collaborative Ultra High Field System (LoCUS), London, UK

[*]E-mail: amer.ajanovic@pmf.unsa.ba

Abstract. The proposed extension to the conventional circuit co-simulation (CCS) method reliably and efficiently introduces arbitrary matching networks into CCS routines and is here dubbed as matching circuit co-simulation (MCCS). It further achieves coil tuning for resonance and an optimum scattering parameters condition that resembles a fully matched coil. Combined with magnetic resonance integral equations (MARIE), the proposed MCCS further accurately produces a full EM simulation of the coils. We first validated MARIE with the MCCS routine to use it to model simple single-channel coils and parallel transmit (pTx) head arrays coupled with Duke, a digital human body model. Having successfully validated the MCCS routine, we swept through both tuning and matching network parameters to optimize the coil. While optimizing for all parameters simultaneously is a viably efficient option for coil models of low complexity, these models are not realistic, and we found that it becomes a highly computationally expensive problem to solve for more complex coil geometries, such as birdcage coils and pTx coils with higher number of channels, especially when shielding is included. Consequently, we separated tuning and matching into two steps, by first tuning the coil to the right frequency, and then introducing matching networks to enhance the power transmission into the body. We observed lower on-diagonal S-parameters after matching in all pTx coils, but 1 coil still had strong cross-coupling. Finally, electromagnetic fields obtained via MARIE for separate port excitation were successfully combined using MCCS.

1. Introduction to the Circuit co-simulation (CCS) techniques

Parallel Transmit Circuit Co-Simulation. RF shimming[1] and parallel excitation[2] in parallel transmit (pTx) coils can be used to address the problems of the RF transmit field (B1+) inhomogeneities and increase the B1+ efficiency inside the body[3–5], in addition to decreasing local SAR values[6,7]. However, simulating pTx coils is more demanding than simulating single-channel coils because

the pTx coils consist of more complex electronic structures with multiple input ports. This leads to a difficulty in optimizing impedance values of several added lumped elements since changing an externally added component value to tune the coil would demand the entire simulation to be rerun. This difficulty in simulating pTx coil arrays while optimizing for the external electronic elements has been overcome over the course of last couple of decades[8,9]. To illustrate, the introduction of exquisitely efficient Kozlov's circuit co-simulation (CCS) for full EM field calculation using S-parameters from a single-port EM simulation with RF circuit investigation for coil element tuning and matching[10] has been an invaluable asset to the community. CCS involves replacing lumped element impedances with additional excitation ports. It results in a seemingly more complex simulation in which many ports are excited; however, since the lumped elements are removed, the structure is not resonant, so the simulations converge more quickly. Once completed, the CCS theory allows for the fields generated from the many-port simulation to be combined to approximate the fields that would be generated if some of those ports were replaced with specific impedance values. The value of CCS lies in the fact that having completed one multi-port simulation, it is then possible to evaluate the coil behavior with various different tuning conditions. The alternative for a complex coil structure is to perform 'resonant' simulations for specific lumped element values – this approach makes optimizing coil properties virtually intractable. CCS, therefore, allows for the optimization of the external coil parameters in tuning, matching, decoupling, and the efficient computation of the full EM fields without having to rerun the multi-port EM simulation for the optimized elements. The further improvements of the CCS method include Zhang's derivation of the S-parameter matrix expression in CCS[11], Lemdiasov's closed-form solution of the same matrix problem to realize the CCS calculations[12], Beqiri's MATLAB implementation of the method with an introduction of optimizable S-parameter's cross-terms for coil decoupling[13].

Tuning, matching, and decoupling. When excited with specific current density, strong coupling or electromagnetic linkage between individual coil elements, especially that of nearest neighbors, is one of the main obstacles in using pTx technology. Moreover, introduction of patients in the scanner leads to further coupling between the coil and the patient, especially at UHF above 7T, where the EM fields' RF wavelength is short and comparable to human tissue dimensions and that of coil[14], so the coupling is even stronger. Consequently, it is challenging to establish stable decoupling between different pTx coil array elements. The community has, therefore, introduced various techniques to reduce strong cross-coupling[8,9,15–17]. However, it is not often clear from literature why certain electronic topologies or lumped element values are more beneficial than the others are. CCS's implementation in MATLAB[13] has proven beneficial in achieving transparent decoupling; however, combining it with magnetic resonance integral equations to efficiently achieve a full EM solution has shown to lead to badly matched coils. Thus, we decided to extend CCS methodology to allow for the introduction of arbitrary matching networks in the optimization routine to achieve more efficient power transfer to the human body, and dubbed it as matching circuit co-simulation (MCCS). Consequently, the novelty behind the MCCS methodology is represented in extending the CCS formalism to incorporate the matching networks into it by producing a closed-form S-parameters solution, which then allowed for efficient coil parameter optimization so the coil models used in MARIE are well tune-and-matched. This further enabled the combination of the MARIE per-port fields for a full EM solution, and further demonstration of the applicability of using MARIE combined with MCCS for other investigative purposes.

2. Matching Circuit Co-Simulation (MCCS) Theory

2.1 CCS Formalism

First, a full 3D EM simulation of the structure being modelled must be run with all of the lumped elements replaced with driving ports. This simulation will produce fields and S-parameters for all ports in the model. To perform the CCS, these S-parameters must be related to those expected for the ports that are driven when a set of defined impedances are placed across the ports corresponding to lumped elements. The array model for the original CCS analysis is given in Fig.1 (left). However, in reality, driving ports have a layer of impedances of their own just like lumped element ports. Then lumped elements network together with the matching elements network account for the final tuning and matching conditions devised to operate a coil at a certain resonant frequency. We, therefore, initially propose adding a layer of matching elements between each driving port and the pre-evaluated coil ports as given in Fig.1 (right). In other words, in our preliminary design, voltage sources (drives D1,D2,…Dnp) are connected to the ports via multiple matching networks, rather than being simply attached to ports as is done in the original CCS. CCS setup (top-left in Fig.1) consists of: power sources (D1…Dp) delivering power straight to the designated driving ports of the coil, whose S-parameters matrix is given by **S**, and lumped elements consisting of imperfect (resistive) capacitors, whose S-parameters matrix is given by **Σ**, attached to the other ports. Matching circuit co-simulation (MCCS) setup (top-right in Fig.1) has the same elements CCS setup has, with an added layer of 2-port T-matching networks (bottom-right), whose S-parameters are given by **M.** Notice that lumped elements in matching networks can be purely capacitive, purely inductive, or both. In terms of the abbreviations used in Fig.1, the capacitance ranges are defined as follows:

- MN Matching C refers to the capacitors in the Matching Network connected in series to the driven port (Cdp);
- MN Series C refers to the capacitors in the Matching Network connected in series to the coil (Csc);
- MN Shunt C refers to the capacitors in the Matching Network connected in parallel (Csh) between the coil and the driven port side.

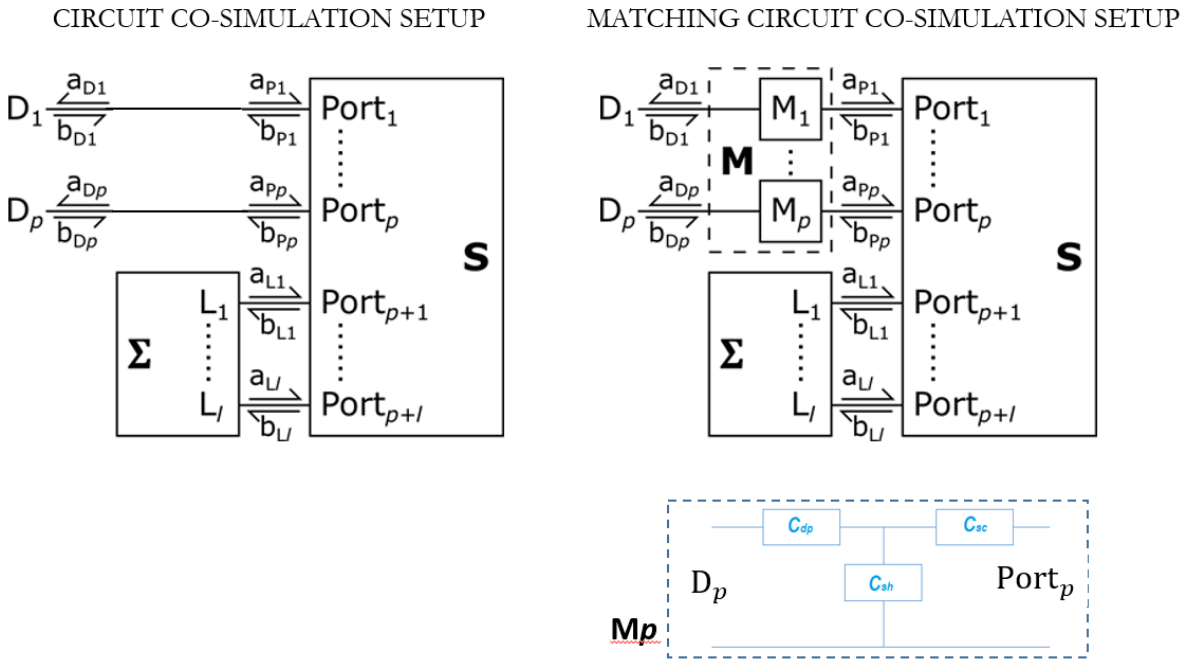

Figure 1: A schematic representation of an RF coil with passive networks.

In both cases, fully pre-evaluated ports S-parameters are described by their S matrix, while the lumped elements network is described by an equivalent S-matrix here called Σ. The matching network's equivalent S-parameters are described by matrix M. Note that each line in the schematics in Fig.1 represents 2 physical transmission lines (1 carrying forward travelling power wave and the other one carrying backward travelling wave). To arrive at the physical S-matrix in both cases, we used signal flow graph theory. The physical S-parameters matrix is defined as the ratio of the reflected power waves to incident power waves as seen from the driving voltage ports.

2.2 MCCS formalism

There are p driven ports to the coil and l lumped element ports, or the artificially/externally added ports consisting of lumped elements, as in the original CCS work. There are a total of l passive components, one for each lumped element port. We introduce further p matching networks, one for each driven port.

Matching Networks. $\mathbf{M}$ is a $2p \times 2p$ matrix of the matching network S-parameters. They are organized into four blocks, each $p \times p$, which group the S-parameters together based on which ports are connected by the S-parameter.

$$\mathbf{M} = \begin{bmatrix} \mathbf{M_{DD}} & \mathbf{M_{DP}} \\ \mathbf{M_{PD}} & \mathbf{M_{PP}} \end{bmatrix} \tag{1}$$

$$\mathbf{M_{DD}} = \begin{bmatrix} \frac{a_{D1}}{b_{D1}} & \cdots & \frac{a_{D1}}{b_{Dp}} \\ \vdots & \ddots & \vdots \\ \frac{a_{Dp}}{b_{D1}} & \cdots & \frac{a_{Dp}}{b_{Dp}} \end{bmatrix}, \mathbf{M_{DP}} = \begin{bmatrix} \frac{a_{D1}}{b_{P1}} & \cdots & \frac{a_{D1}}{b_{Pp}} \\ \vdots & \ddots & \vdots \\ \frac{a_{Dp}}{b_{P1}} & \cdots & \frac{a_{Dp}}{b_{Pp}} \end{bmatrix}, \mathbf{M_{PD}} = \begin{bmatrix} \frac{a_{P1}}{b_{D1}} & \cdots & \frac{a_{P1}}{b_{Dp}} \\ \vdots & \ddots & \vdots \\ \frac{a_{Pp}}{b_{D1}} & \cdots & \frac{a_{Pp}}{b_{Dp}} \end{bmatrix}, \mathbf{M_{PP}} = \begin{bmatrix} \frac{a_{P1}}{b_{P1}} & \cdots & \frac{a_{P1}}{b_{Pp}} \\ \vdots & \ddots & \vdots \\ \frac{a_{Pp}}{b_{P1}} & \cdots & \frac{a_{Pp}}{b_{Pp}} \end{bmatrix} \tag{2}$$

$\mathbf{M_{DD}}$ is a $p \times p$ matrix of voltage scattered from the driven side of the matching networks by voltage incident on the driven side of the matching networks; $\mathbf{M_{DP}}$ is a $p \times p$ matrix of voltage scattered from the driven side of the matching networks by voltage incident on the coil side of the matching networks; $\mathbf{M_{PD}}$ is a $p \times p$ matrix of voltage scattered from the coil side of the matching networks by voltage incident on the driven side of the matching networks; $\mathbf{M_{PP}}$ is a $p \times p$ matrix of voltage scattered from the coil side of the matching networks by voltage incident on the coil side of the matching networks.

In the case that each matching network is an independent 2-port network, each block is a diagonal matrix of p S-parameters of the same type (S_{11}, S_{12}, etc.) of each matching network:

$$\mathbf{M} = \begin{bmatrix} \mathbf{M_{DD}} & \mathbf{M_{DP}} \\ \mathbf{M_{PD}} & \mathbf{M_{PP}} \end{bmatrix} = \begin{bmatrix} \begin{bmatrix} M1_{11} & & 0 \\ & \ddots & \\ 0 & & Mp_{11} \end{bmatrix} & \begin{bmatrix} M1_{12} & & 0 \\ & \ddots & \\ 0 & & Mp_{12} \end{bmatrix} \\ \begin{bmatrix} M1_{21} & & 0 \\ & \ddots & \\ 0 & & Mp_{21} \end{bmatrix} & \begin{bmatrix} M1_{22} & & 0 \\ & \ddots & \\ 0 & & Mp_{22} \end{bmatrix} \end{bmatrix} \tag{3}$$

Coil. $\mathbf{S}$ is a $(p + l) \times (p + l)$ matrix of the coil S-parameters. It is likewise organized into four blocks, but these are of different sizes. Additionally, the four component matrices are not diagonal:

$$\mathbf{S_{PP}} = \begin{bmatrix} \frac{b_{P1}}{a_{P1}} & \cdots & \frac{b_{P1}}{a_{Pp}} \\ \vdots & \ddots & \vdots \\ \frac{b_{Pp}}{a_{P1}} & \cdots & \frac{b_{Pp}}{a_{Pp}} \end{bmatrix}, \mathbf{S_{PL}} = \begin{bmatrix} \frac{b_{P1}}{a_{Pp+1}} & \cdots & \frac{b_{P1}}{a_{Pp+l}} \\ \vdots & \ddots & \vdots \\ \frac{b_{Pp}}{a_{Pp+1}} & \cdots & \frac{b_{Pp}}{a_{Pp+l}} \end{bmatrix}, \mathbf{S_{LP}} = \begin{bmatrix} \frac{b_{Pp+1}}{a_{P1}} & \cdots & \frac{b_{Pp+1}}{a_{Pp}} \\ \vdots & \ddots & \vdots \\ \frac{b_{Pp+l}}{a_{P1}} & \cdots & \frac{b_{Pp+l}}{a_{Pp}} \end{bmatrix}, \mathbf{S_{LL}} = \begin{bmatrix} \frac{b_{Pp+1}}{a_{Pp+1}} & \cdots & \frac{b_{Pp+1}}{a_{Pp+l}} \\ \vdots & \ddots & \vdots \\ \frac{b_{Pp+l}}{a_{Pp+1}} & \cdots & \frac{b_{Pp+l}}{a_{Pp+l}} \end{bmatrix} \quad (4)$$

$\mathbf{S_{PP}}$ is a $p \times p$ matrix of voltage scattered from the excited coil ports by voltage incident on the driven coil ports; $\mathbf{S_{PL}}$ is a $p \times l$ matrix of voltage scattered from the excited coil ports by voltage incident on the lumped element coil ports; $\mathbf{S_{LP}}$ is a $l \times p$ matrix of voltage scattered from the lumped element coil ports by voltage incident on the driven coil ports; $\mathbf{S_{LL}}$ is a $l \times l$ matrix of voltage scattered from the lumped element coil ports by voltage incident on the lumped element coil ports. Finally, that way, the coil S-parameter matrix becomes:

$$\mathbf{S} = \begin{bmatrix} \mathbf{S_{PP}} & \mathbf{S_{PL}} \\ \mathbf{S_{LP}} & \mathbf{S_{LL}} \end{bmatrix} = \begin{bmatrix} \begin{bmatrix} S_{1,1} & \cdots & S_{1,p} \\ \vdots & \ddots & \vdots \\ S_{p,1} & \cdots & S_{p,p} \end{bmatrix} & \begin{bmatrix} S_{1,p+1} & \cdots & S_{1,p+l} \\ \vdots & \ddots & \vdots \\ S_{p,1} & \cdots & S_{p,p+l} \end{bmatrix} \\ \begin{bmatrix} S_{p+1,1} & \cdots & S_{1,p} \\ \vdots & \ddots & \vdots \\ S_{p+l,1} & \cdots & S_{p+l,p} \end{bmatrix} & \begin{bmatrix} S_{p+1,p+1} & \cdots & S_{p+1,p+l} \\ \vdots & \ddots & \vdots \\ S_{p+l,p+1} & \cdots & S_{p+l,p+l} \end{bmatrix} \end{bmatrix} \quad (5)$$

Lumped Elements. $\mathbf{\Sigma}$ is an $l \times l$ matrix of the lumped elements' S-parameters:

$$\mathbf{\Sigma} = \begin{bmatrix} \frac{a_{L1}}{b_{L1}} & \cdots & \frac{a_{L1}}{b_{Ll}} \\ \vdots & \ddots & \vdots \\ \frac{a_{Ll}}{b_{L1}} & \cdots & \frac{a_{Ll}}{b_{Ll}} \end{bmatrix} \quad (6)$$

If the ports are not interconnected, the $\mathbf{\Sigma}$ matrix is diagonal:

$$\mathbf{\Sigma} = \begin{bmatrix} \mathbf{\Gamma}_1 & & 0 \\ & \ddots & \\ 0 & & \mathbf{\Gamma}_l \end{bmatrix} \quad (7)$$

$\mathbf{\Gamma_n}$ is the reflection coefficient of the nth lumped element, as given by: $\mathbf{\Gamma_n} = \frac{Z_{L1} - Z_0}{Z_{L1} + Z_0}$, where Z_0 is the characteristic impedance used to analyse the networks (typically 50 Ω).

Using the Matrix Signal Flow Graph approach, as shown in Fig.2, it is simple to verify the CCS result from Beqiri, et al.[13 18]. $\mathbf{S^{CCS}}$ is the S-matrix of the coil ports without the matching network and is valid within MCCS:

$$\mathbf{S^{CCS}} = \mathbf{S_{PP}} + \mathbf{S_{PL}}\mathbf{\Sigma}(\mathbf{I} - \mathbf{S_{LL}}\mathbf{\Sigma})^{-1}\mathbf{S_{LP}} \quad (8)$$

When the matching network is added, one can arrive at the following expression for $\mathbf{S^{MCCS}}$, the physical S-parameters matrix of the matched coil:

$$\mathbf{S^{MCCS}} = \mathbf{M_{DD}} + \mathbf{M_{DP}}\mathbf{S^{CCS}}\left(\mathbf{I} - \mathbf{M_{PP}}\mathbf{S^{CCS}}\right)^{-1}\mathbf{M_{PD}} \quad (9)$$

2.3 Using MCCS in Coil Tuning-and-Matching and for Full EM Field Simulation

The lumped elements in the tuning networks and the matching networks can be varied so as to minimize S-parameters or optimize them under specific conditions to tune the coil to the correct frequency, match it to the transmission line impedance of 50 Ohms for the most effective power

transfer to the body, and decouple the coil to reduce the cross-talk between different driving channels and reduce power losses to the surroundings. Upon finalizing tuning-and-matching and obtaining the optimal working conditions for the coil under investigation, it is possible to combine the MARIE-produced fields evaluated per each excited port with the usage of MCCS. If a coil has a total of N_p ports, and if we denote by E_{pp} and B_{pp}, respectively, the electric and magnetic fields obtained when each port of an N_p-port coil is excited separately (with 'pp' in the subscript standing for 'per port'), then using the full power wave vector $\boldsymbol{a}$ obtained via MCCS calculation for the selected set of tune-and-matching parameters, the full EM field solutions are then simply:

$$B_{full} = B_{pp}a = \sum_{k=1}^{N_p} B_{pp\,k} \cdot a_k \quad \text{and} \quad E_{full} = E_{pp}a = \sum_{k=1}^{N_p} E_{pp\,k} \cdot a_k \tag{10}$$

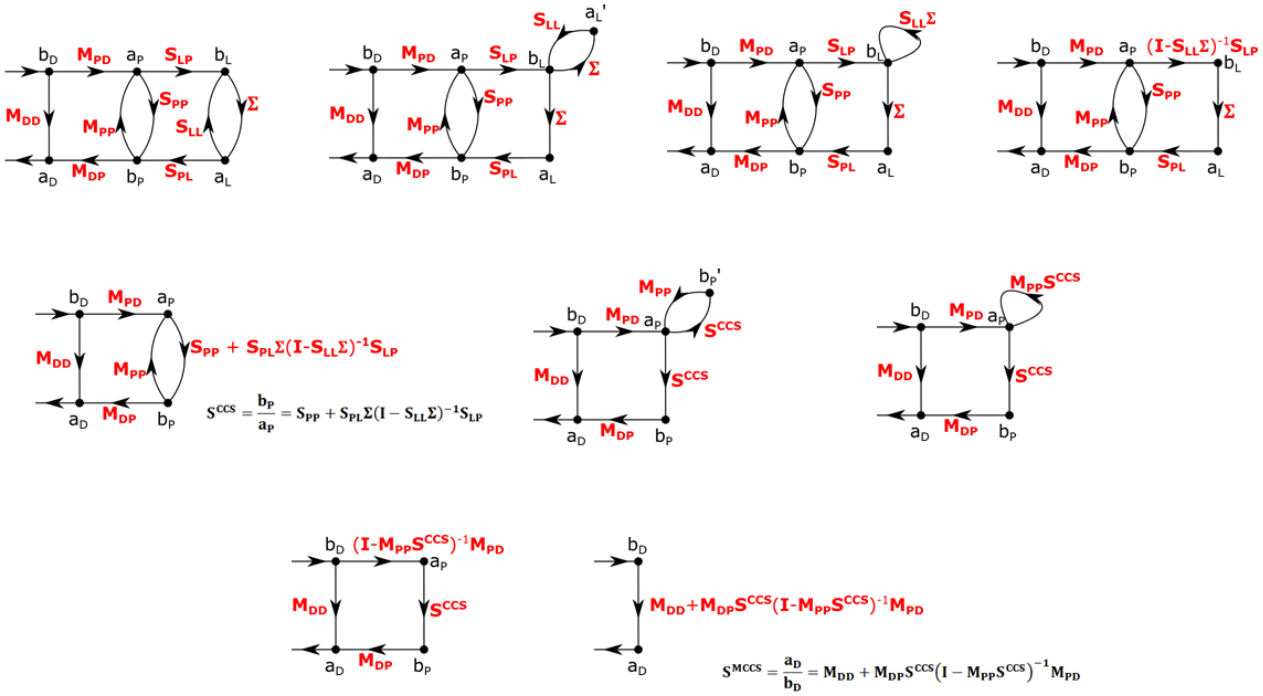

Figure 2: Demonstration of the matching circuit co-simulation derivation using matrix signal flow graphs.

3. Methods in validating MCCS and demonstrating its usage with MARIE

Initially, tuning and matching of more simplistic coil models was done by varying all parameters of the lumped element networks and matching networks simultaneously to find a global minimum. That, however, becomes a computationally expensive problem to solve when applied to more realistic coil types due to its multi-dimensional nature. Consequently, we introduced a cost function consisting of S-parameters and subjected it to linear constraints to minimize it by optimizing matching network elements. The method's accuracy was tested on the 1-channel and 4-channel loop arrays and compared to the CCS results when the conditions should lead to equivalent results, i.e. when the series branch in each of the T-shaped 2-port matching elements is short-circuited, and the shunt branch is open-circuited. MCCS was further combined with MARIE[19] to demonstrate applicability to full simulation of 4 realistic coil types coupled with human body models. The following sections introduce more structured explanations of the methodologies used:

1 MATLAB MRGF implementation for Duke body model;
2 The coil simulation setup**;**
3 MCCS Self-Validation with respect to CCS using a 1-Tx coil;
4 MCCS optimization for efficient tuning-and-matching of realistic pTx coil models;
5 Quadrature Mode B1+: combining MARIE per-port fields with MCCS.

3.1 MATLAB MRGF implementation for Duke body model

The described routines were applied in MATLAB with the numerical experiments executed on a Linux server machine, supplied with a Dual Intel Xeon E5- 2670 v3 CPU processor operating at 2.3 GHz enhanced by an Nvidia Corporation GP102 (Titan Xp) GPU card with 12 GB allocated memory running at 11 Gbps. The experiments' performances were accelerated using MATLAB's Parallel Toolbox, with a maximum of 12 simultaneous processes enacted in parallel. The operation frequency used in the experiments was 298MHz (MRI-equivalent of 7T). All numerical experiments focused on 1 digital human body model, which was the Duke body model from Virtual Model family[20]. The body model was centrally surrounded by a cylindrical excitation coil domain of $\mathbf{130mm} < \boldsymbol{r} < \mathbf{210mm}$, $|\boldsymbol{z}| \leq \mathbf{300mm}$ (see Fig.3, far left). To produce the interpolation points and the set of MRGFs for the body model, we used an implementation of the MRGF-generation routine as described in the original MARIE work[19] with a few modifications, by utilizing randomized singular value decomposition (RSVD) tolerance of 10^{-1}, and volumetric integral equation solver (VIE) tolerance of 10^{-3}. The spatial resolution was set to **5mm** on a grid of 128x128x139 voxels. The time needed to compute the interpolation points and the MRGFs was 13.3h. The produced matrix sizes and execution times are summarized in Table 4.1.

Table 1: Dimensions of matrices constituting the created MRGFs, their computation times, and computation times of full EM solution when the MRGFs are coupled with the 5 coil models shown in Fig.3.

	MRGFs		**Coil**	Solving **VIE + MCCS [min]**
IdxS	15625x3		1n	1.3
IdxI	12172x3			
Dcoord	1950x3		2n	3.1
P	911943x5850			
Um	5850x723		2s	6.2
Sm	723x723			
Vm	5850x723		8n	10.1
X	723x5850			
M	911943x723		8s	13.0
Uin	911943x723			
MRGF Computation Time	**13.3h**		**Total**	**33.7**

3.2 The coil simulation setup

Figure 3 shows the representation of the body-coil configurations used throughout this study. After placing the Duke body model inside the MRGF excitation domain (green in Fig.3, far left) and obtaining the MRGFs, they were combined with different coil structures (red in Fig.3) modelled by using MARIE's built-in GUI[19] functionality that utilizes GMSH routines to generate a tetrahedral tessellation of the object for surface integral formalism[21]. The designed coil models were all made out of copper (resistivity $\frac{1}{\sigma_c} = 1.7 \cdot 10^{-8}\Omega\text{m}$) with the following specifications:

Coil **1n**: Single-channel 6-port rectangular planar loop coil, with no shield, with 1 port on the top, 1 on the bottom side, and 4 others distributed evenly on the other 2 sides;
Coil **2n**: 2-channel 32-port birdcage coil, with no shield, as the first realistic coil example used;
Coil **2s**: shielded 2-channel 32-port birdcage coil;
Coil **8n**: 8-channel 32-port pTx coil, consisting of 8 4-port planar loops, with each port located at the centre of each of its sides;
Coil **8s**: shielded 8-channel 32-port pTx coil.

The fields per port results were obtained utilizing the direct volumetric surface integral equation (VSIE-direct) solver at tolerance 10^{-3}. Finally, a couple of tuning and matching element optimization routines within MCCS were applied to tune the coil the coil to 298MHz and match it to 50Ω, after which the elements were fixed and MCCS was used to obtain the full-wave EM solutions. The optimization routines are explained briefly in the following sections.

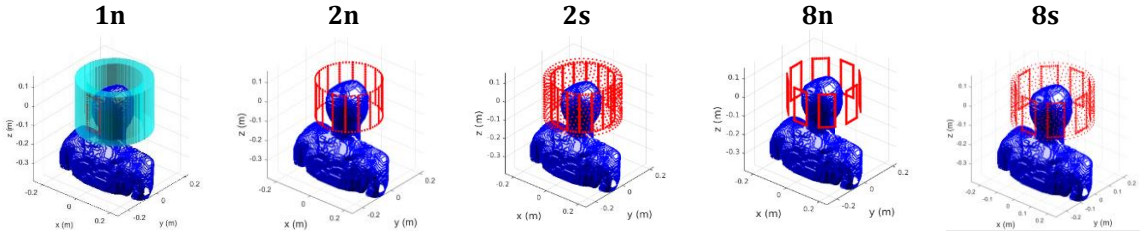

Figure 3: Coil structures used throughout this thesis. Left – Right: Body-coil-excitation domain configuration. Duke body model (dark blue) is placed inside the MARIE MRGF excitation domain (green), in which the coil structures (red) are excited. Coil models used are (from left to right): Single-channel rectangular planar loop coil with no shield (**1n**); 2-channel birdcage coil with no shield (**2n**); shielded 2-channel birdcage coil (**2s**); 8-channel pTx coil with no shield (**8n**); shielded 8-channel 32-port pTx coil (**8s**).

3.3 MCCS Self-Validation with respect to CCS using a 1-Tx coil

The self-validation portion of the study was done via the concept of tuning and comparing the results of tuning with CCS to tuning with MCCS. The conventional way of tuning consists of sweeping through various frequencies of the coil input signal, but MARIE is a frequency-domain solver, so we solved for only one frequency. Hence, instead of sweeping through multiple frequencies, we swept through the impedance values to make the coil resonant at the frequency of interest. Therefore, tuning the single-channel coil (1n) to 298 MHz and matching it to 50Ω reference impedance via MCCS was done by including the following variable electronic elements. First, the lossy capacitors (R=1Ω) as lumped elements were attached to all non-excited ports. These capacitors can be defined as break-up capacitors (Cbu). The driving port, on the other hand, had a T-matching network attached to it (see Fig.1) consisting of 3 different capacitances: the parallel (shunt) capacitance (Csh), the coil-side series capacitance (Csc) and the series capacitance attached to the driven port (Cdp). Hence, tuning and matching was performed by sweeping S11-parameters across Cbu, Csh, Csc, Cdp in the range of [0.1-10]pF with 100 samples each, to find the global minimum S11 for resonance condition. We then applied MCCS on single channel coil as a self-validation study with respect to the conventional CCS. Here S11-parameters obtained using CCS were compared to the S11-parameters obtained for the case where the series branches of the matching network attached to the driving port were short-circuited and parallel branch open-circuited. That in effect eliminates the matching network from the RF circuitry, so the conditions obtained should be equivalent to those obtained by using conventional CCS to sweep through the lumped capacitors in finding the global minimum. The lumped element capacitances were selected to be in the range of [0.1-10]pF with 1000 samples. Upon fixing all capacitive network parameters, the coil was considered tune-and-matched.

3.4 MCCS optimization for efficient tuning-and-matching of realistic pTx coil models

While minimizing S-parameters function for a plethora of matching and tuning elements was still computationally effective to an extent for simpler coil models, it became computationally exhaustive in addressing larger, electronically more complex, but more realistic coil designs, such as 2n, 2s, 8n, 8s, used here. Therefore, to reduce the dimensionality of the problem, we devised a 2-step tuning-and-matching protocol, in which, tuning was done by simply open-circuiting the shunt elements of the matching network, short-circuiting the series elements (thus eliminating the matching network as in section 3.3) and sweeping through the lumped capacitors to tune the coil to the right frequency. The second step consisted of fixing all the lumped capacitors at the values found after tuning to the correct frequency and then optimizing the matching network elements until a constrained minimum of a cost function is found. Matching network elements here were defined as pure complex numbers; in other words, we assumed each branch of the 2-port T-shaped network could contain both capacitors and inductors, so the optimization then reduced to finding optimum inductor values L and capacitive values C in the matching networks. The cost function consisted of the estimated S-parameter diagonal values using MCCS form, as summarized below:

$$cost(z) = \left\| diag\left(S_{mccs}(z)\right) \right\| \tag{11}$$

$$z = j2\pi fl + \frac{1}{j2\pi fc} \tag{12}$$

The optimized solution is then:

$$\hat{z} = \arg\min\{cost(z)\} \tag{13}$$

Notice that l and c used here are just generic vector notations for inductivity and capacitance of the matching networks. They refer to all 3 branches of the matching 2-port T-network.

The optimum impedance parameters $\hat{z}$ consist of the real and imaginary values of each individual branch in the matching network attached to driving ports, with an assumption that the elements optimizing the coil are the same. Consequently, while there was a total of 2x3x2=12 $\hat{z}$ parameters for the 2-channel birdcage coils and 2x3x8=48 $\widehat{z_8}$ parameters for the 8-channel pTx coils to optimize, by assuming the same matching networks on all driving ports, we reduced the optimization problem to just 6 parameters: inductors in series with the excitation or driving power side (L_{dp}), capacitors in series with the driving power side (C_{dp}), inductors in series with the coil side (L_{cs}), capacitors in series with the coil side (C_{cs}), shunt inductors in parallel branch within the matching network (L_{sh}) and the shunt capacitors (C_{sh}). These could then be estimated with the help of the constrained optimization, as given below:

$$\hat{z} = \arg\min\left\{cost\left(j2\pi fl + \frac{1}{j2\pi fc}\right)\right\} \tag{14}$$

$$l \in \left\{L: L_{k\ lower} < l_k < L_{k\ upper}, k = 1,2,3\right\}$$

$$c \in \left\{C: C_{k\ lower} < c_k < C_{k\ upper}, k = 1,2,3\right\}$$

The lower and upper bounds on the inductors were set to $L_{k\ lower} = 10$ nH and $L_{k\ upper} = 3000$ nH, respectively, while the lower and upper bounds on the capacitors were set to $C_{k\ lower} = 1.5$ pF and $C_{k\ upper} = 30$ pF, respectively.

We repeated this process 20 times within a multi-start approach and selected the conditions giving out the smallest of the cost function minima. The constrained optimization itself was solved with the help of one of MATLAB's Optimization Toolbox protocols. We used a nonlinear programming solver ('fmincon') using the 'interior-point' algorithm as the optimization solver and multi-start approach to search for the optimal matching network parameters within the preselected bounds.

3.5 Quadrature Mode B1+: combining MARIE per-port fields with MCCS.

Upon finalizing tuning-and-matching and obtaining the optimal working conditions for the coil under investigation, we combined the MARIE fields evaluated per each excited port with the usage of MCCS. Let Epp and Bpp denote the electric and magnetic fields obtained when each port of a 32-port coil is excited separately. Using the full power wave vector $\boldsymbol{a}$ obtained via MCCS for the selected set of tune-and-matching parameters, the full EM field solutions are then simply:

$$B_{full} = B_{pp}a = \sum_{k=1}^{32} B_{pp\,k} \cdot a_k \quad \text{and} \quad E_{full} = E_{pp}a = \sum_{k=1}^{32} E_{pp\,k} \cdot a_k \tag{15}$$

For single-channel coils, the full solution would be of the dimensions: $Nx \times Ny \times Nz \times 3$ (where 3 is for all 3 principal axis components), while for the pTx coils, it is: $Nx \times Ny \times Nz \times 3 \times Nc$, where Nc denotes the number of channels or driving ports. For 2n and 2s, $Nc = 2$, while for 8n and 8s, $Nc = 8$.

Defining B_{1x} and B_{1y} as the x- and y-components of the full magnetic field, they can then just be explicitly written as the 1st and 2nd components of the 4th dimension in the full solution obtained via MARIE+MCCS:

$$B_{1x} = B_{full}(:,:,:,1,:), B_{1y} = B_{full}(:,:,:,2,:) \tag{16}$$

So, the transmit magnetic field (B1+) then simply becomes:

$$B_1^+ = \frac{B_{1x} + jB_{1y}}{2} \tag{17}$$

Ultimately, the focus of this study was on a specific combination of the channel fields in relation to power distribution. Therefore, we applied correctional phase terms on each channel of the coils we examined to undo the effects of physical phase each channel was in with respect to others, so that the channels would be in phase, so maximally efficient circularly polarized (or quadrature mode) B1+ field would be established within the mid-slice in the head. The combination of such phases was stored for 4 realistic coils. The 2 driving ports on each of the two birdcage coils (2n and 2s) were selected to be on the top ring at the back of the head, 90 degrees away from each other on the ring (ports 7 and 11), while the driving ports on each of the two 8-channel pTx coils (8n and 8s) were selected to be each top port on 8 individual coils within the array (ports 1,5,9,13,17,21,25,29). Finally, full electric field solutions were used to evaluate specific absorption rate (SAR) normalized with respect to input power, as described in the literature.

4. Results and Discussion

4.1 MATLAB MRGF implementation for Duke body model

The Duke MRGF matrices were generated successfully following MARIE's "offline" stage within 13.2 hours. Duke voxelization and excitation domains were applied on the grid which resulted in a total of 126x126x139=2206764 voxels or 6620292 degrees of freedom (DOFs). Duke occupied 971106 voxels, and the rest pertained to the air voxels. The excitation domain took up 328644 voxels, leading to 328644x3=985932 current dipole components. The generated incident field basis, following RSVD and discrete empirical interpolation (DEIM) routines, relied on 788 basis vectors and 1519 DEIM coordinates. MARIE's main acceleration feature is the MRGF matrices that include DEIM coordinates, which represent points at which the fields are evaluated to achieve the best possible accuracy and here stand for 971106/1519=639 times reduction with respect to total body voxels at no cost of accuracy[22–24]. This is in similar agreement with Villena's work[19] and further implementations[25–31].

4.2 The coil simulation setup

The offline phase was not fast but was executed just once and was coil-independent. On the other hand, the online phase consisting of MARIE solvers, by which the impedance parameters Zp, coil and body port currents (Jcp, Jbp) as well as fields per port are evaluated, was much faster and was utilized with our 5 coil models. MCCS routine was quick and lasted 192 microseconds per capacitance sweep. Single channel configuration was solved within just 9 seconds for volumetric body current J and E fields and a further 80 seconds for B field per excited port. This was increased up to 1.3 min and 5.6 min when calculating J-E and B, respectively, for our pTx coil models, depending on the complexity. The computation times and matrix sizes are summarized in Table 1, and one can notice that the more electronically complex the coil model, the higher the execution time, as expected, and as reported across several other studies implementing MARIE[19,23–25,28–30,32].

4.3 MCCS Self-Validation with respect to CCS using a 1-Tx coil

The resulting S11 vs break-up capacitance (Cbu) curves for the conventional CCS and the proposed MCCS are shown in Fig.4 along with the error metric. One can note that the CCS and MCCS curves are barely distinguishable, which is further solidified by the relative error metric being in the range [-0.025,0.025]%. This is expected as short-circuiting the series branches in matching networks and open-circuiting the shunt branches effectively eliminates matching networks from the RF coil circuitry, so the MCCS-predicted S-parameters should reduce to those predicted by CCS.

The shape of S11 for single channel coil and the S11 minimum of -80 dB demonstrates a better-than-perfect match, which is also unnecessary, and so the capacitance can be fixed at the values reflecting more realistic matching scenarios. It should be noted that the short-circuit and open-circuit conditions in the matching network in the self-validation study were not ideal either. The matching network impedances were selected to be such to lead to an equivalent solution as if we were solving the problem using the traditional CCS, i.e. $Z_{dp} = -\frac{j}{2\pi f C_{dp}} \approx 0$ (short − circuit) $\Leftrightarrow$ $C_{dp} = 100$ nF. The same capacitance value was taken for the series impedance on the coil side, i.e. $C_{sc} = 100$ nF. The shunt matching impedance is $Z_{sh} = -\frac{j}{2\pi f C_{sh}} \approx \infty$ (open − circuit) $\Leftrightarrow$ $C_{sh} = 1 \times 10^{-18}$ F. These selected capacitance values are far from ideal; however, they were plausibly realistic, and the results show that they lead MCCS to a solid approximation of the CCS, but not an ideal match, as expected. Therefore, this means that under these conditions, our MCCS method can still be used as the conventional CCS method, that is, without the matching network, and return the same results as the CCS.

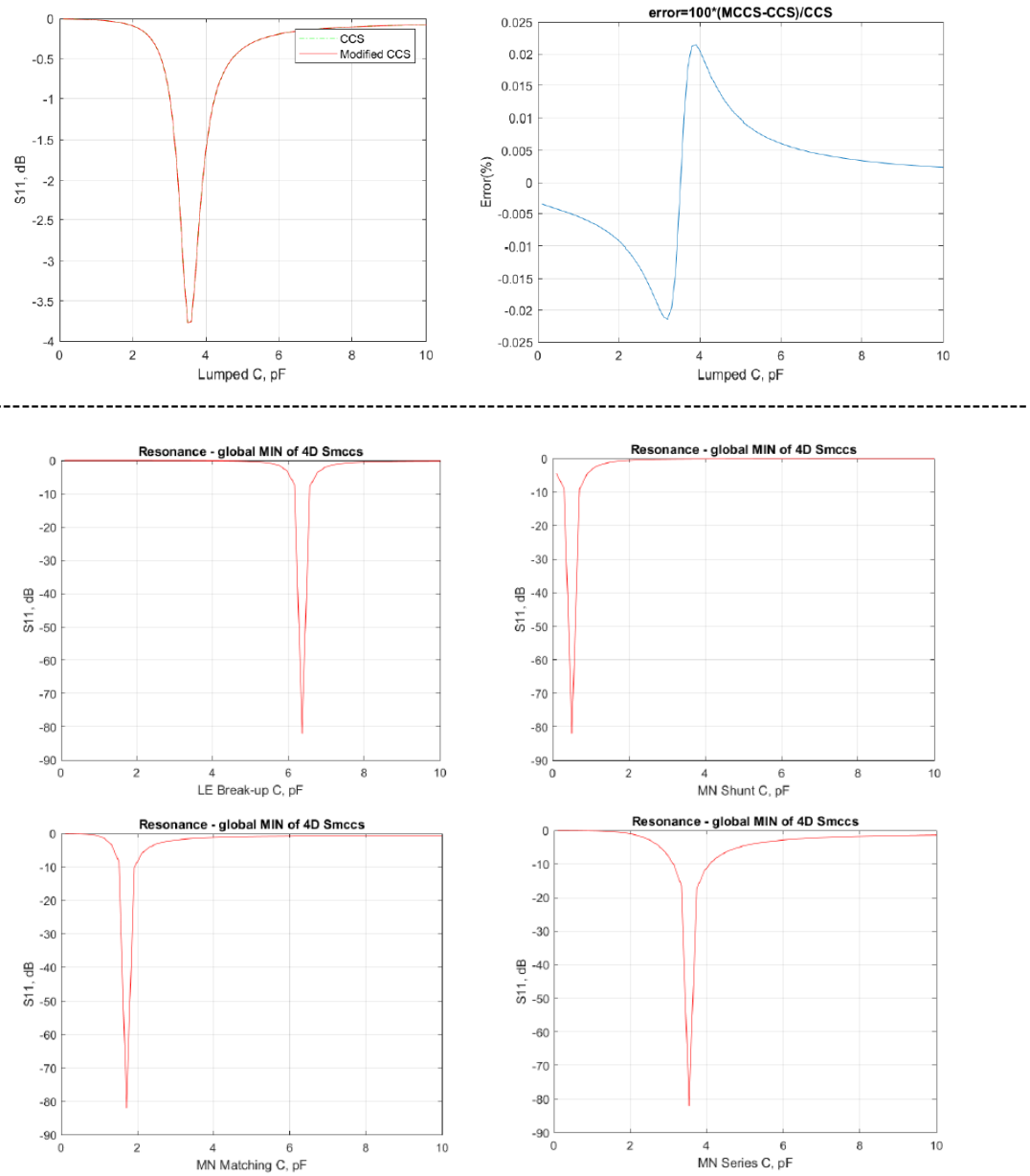

Figure 4: **Single-channel coil validation and application:** Tuning and matching by minimizing MCCS-produced S-parameters. Top: Self-validation test – comparison of CCS results to MCCS when the matching elements in the T-network are such that the series branches are short-circuited, while the shunt (parallel) branch is open-circuited via a direct plot (Top-Left) and via a relative error metric (Top-Right) – notice the results being indistinguishable as expected. (Bottom): S11 curves obtained via finding global minimum of the MCCS-produced S-parameters for the single-channel coil at resonance.

4.4 MCCS optimization for efficient tuning-and-matching of realistic pTx coil models

Tuning. Figure 5 shows the results of the 2-step tuning-and-matching, consisting of sweeping through the tuning capacitors to find the S-parameters local minimum corresponding to CP-mode when no matching networks are attached for tuning, and constrained optimization of the matching parameters for matching once the tuning capacitors are fixed. One should notice that for the birdcage coil models, the S11 parameters shown in the top row of Fig.5 while tuning contain end-ring resonances (peaks) that do not correspond to the CP-mode. Further investigation showed that the only capacitor tuning the birdcage coil structures into a resonant

frequency of 298MHz that would also give out the CP-mode in B1+ field was the 2nd peak from the right for both of the birdcage coils (2n and 2s). The absolute minimum in the case of birdcage coils does not correspond to the CP-mode, and hence the coil was tuned 'manually' using the capacitor corresponding to the 2nd peak from the right in the S11 parameters curve. This is in similar agreement with Malik et al. study on neonates' safety[33], where the authors used a shielded birdcage coil structure with same dimensions, but applied a wide-band excitation across different frequencies to tune the coil to the 7T-equivalent one. The 8-channel coils tuning was straightforward as indicated in Fig.5; the global minimum of the Snn-parameters corresponds to the resonant condition that gives out the CP-mode. One can notice from all S11 curves in the top row of Fig.5 that the return loss was rather high, so matching would be necessary.

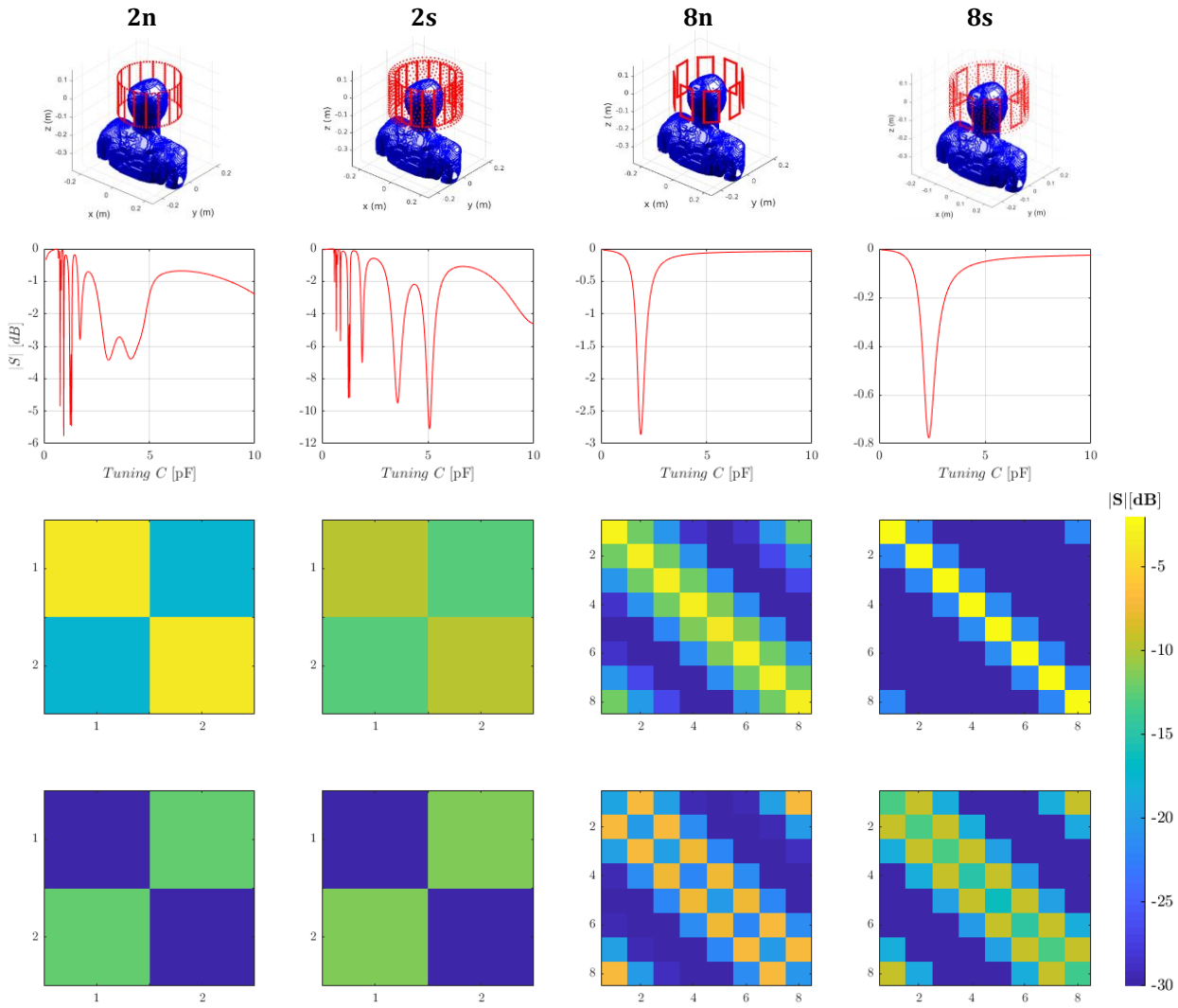

Figure 5: **4 realistic pTx coil models** (1st row at the top): Tuning and matching in a 2-step process. Tuning was performed first by varying the lumped capacitor values to estimate Snn-parameters (2nd row from the top), after which the tuning capacitance was fixed to the correct mode of operation to give out all S-parameters before matching (3rd row), and finally the MCCS-produced Snn-parameters were minimized subject to linear constraints, to give out lower overall S-parameters (4th row). Notice there is still strong coupling between the nearest coil elements, particularly for the 8-channel pTx coil (8n). The 4 coil models used are (from left-right): 2-channel birdcage coil (2n), shielded 2-channel BCC (2s), 8-channel pTx (8n), and shielded 8-channel pTx coil (8s).

Matching. The bottom 2 rows in Fig.5 show the full S-parameters matrices for all 4 realistic coil models before and after matching networks were introduced into tuning. Focusing on the on-diagonal S-parameters, one can notice that adding matching clearly reduces the Snn parameters from -5dB level to -20dB level, so in theory, the power from the coil should be transmitted to the body much more efficiently. However, focusing on the cross-terms or off-diagonal S-parameters, which signify the situation in which the power is sent from one channel, but exits by another channel of the coil, one can notice there was strong coupling associated between the channels, especially the nearest neighbours. To illustrate, most of the coils reported an increase in return loss between the coil's adjacent elements. For instance, the 2n coil showed an increase from -17dB to -12dB in S12 parameters, which is not ideal, considering it means that the power we were aiming to transmit to the body was now being retransmitted through the other channel of the coil. In other words, the figure indicates that the power went into one channel, but then went back down the line from another port, so it was effectively lost. This is one of the main limitations of the coil models evaluated, which do not have any natural decoupling methods implemented. These could be overlap decoupling circuits or capacitive networks that could then be added into the MCCS routine to optimize their parameters and allow for better decoupling. Furthermore, one other limitation of the proposed usage of the MCCS method in optimizing coil parameters is its inability to account for decoupling circuits that would minimize the cross-talk between adjacent coil elements. One simple way to address this would be to expand our cost function to not only consider minimizing the on-diagonal S-parameters, but rather all S-parameters without adding any external circuits, but optimizing for the existing elements of the matching networks while focusing on all S-parameters instead of just on-diagonal ones. A similar approach to this was done in the Beqiri study[18]. Still, the reported values on both on-diagonal (Snn) and off-diagonal (Snm) parameters were well within the range of reported values in the literature.

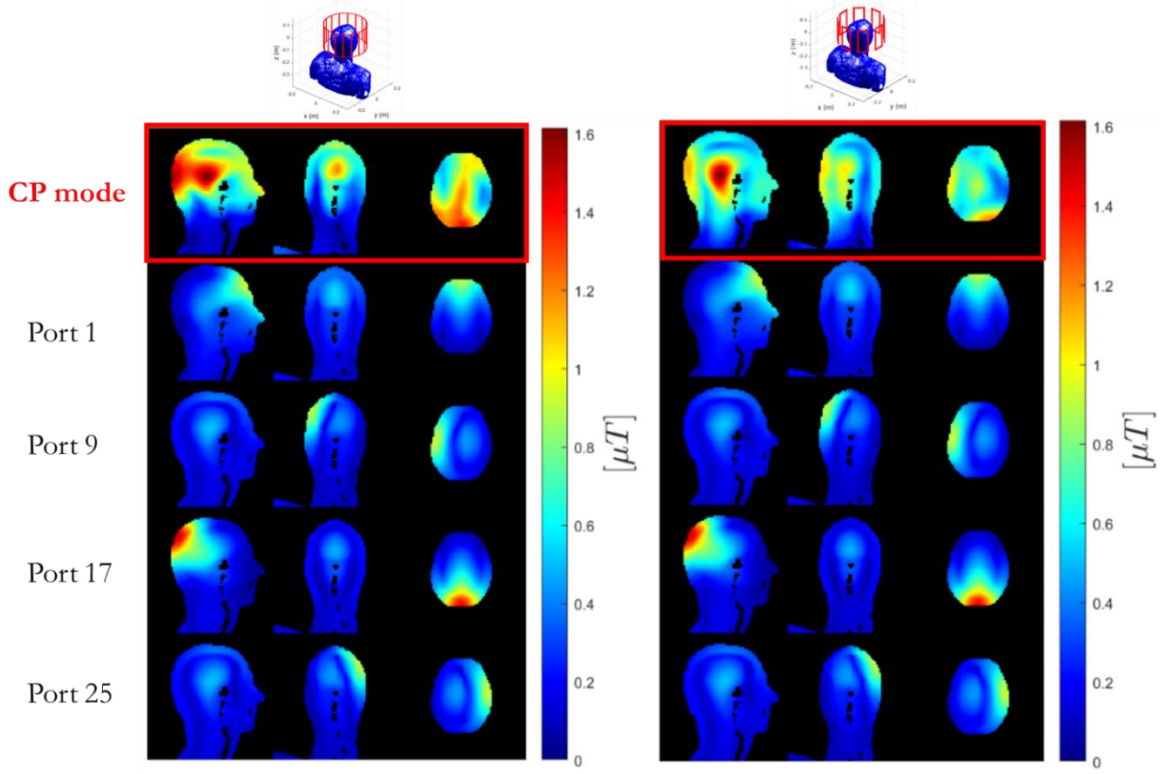

Figure 6: Demonstration of using MCCS to combine EM fields in body obtained via MARIE for each excited port element into total fields per each excited driving port (or per each channel), to then use those to obtain the quadrature mode (or circularly polarized, CP mode) B1+. Left: 2-channel birdcage coil (2n); Right: 8-channel pTx coil (8n).

4.5 Quadrature Mode B1+: combining MARIE per-port fields with MCCS

The B1+ maps per each 4 selected excitation ports of the 2 selected realistic coils without shields (2n, 8n) are shown in Fig.6. It is worth noting that there is a total of 32 B1+ maps produced with unitary electric field excitation across the port gap by MARIE on each of the 32 ports in any realistic coil structure examined here. These 32 per-port B1+ fields were combined using MCCS for the specified tuning-and-matching conditions to lead to B1+ maps for each driving port of the coil structure. That way, these 32 per-port B1+ fields combined into only 2 maps of B1+ fields, each per one of the 2 driving ports in the birdcage coil structures, while there was a total of 8 B1+ maps per channel (each one a composite of 32 per-port B1+ fields) for the 8-channel pTx coil structures. Furthermore, the phases were then imposed on the driving conditions of every port power wave in such a way to maximize the B1+ field inside a preselected central region of a mid-head slice, or to form the CP-mode B1+ (cpB1+). It is noticeable from Fig.6 that each cpB1+ is well defined within the central region, as expected.

4.6 Limitations

It is obvious from the presented results that the main limitation of our study is strong coupling still present after the 2-step tuning and matching routine introduced here. The method that addresses decoupling the most comprehensively is Li's circuit spatial optimization (CSO)[8]. The study introduces methods to enable the modeling and optimization of decoupled circuits within a double-row transmit and receive head coil array by deriving a closed-form S-parameter matrix of the coil array that has tuning, matching, and decoupling circuits. Therefore, CSO revealed limitations in our MCCS method, and directions in which it can be further improved.

Firstly, the inability to include decoupling circuits in estimating S-parameters is a drawback of the proposed MCCS method, so enabling the introduction of separate decoupling matrices into the whole MCCS routine, would allow for an extra set of parameters to optimize, and lead to better operating coil conditions. Rather than introducing an extra set of parameters through decoupling circuits, another and much simpler way to improve our method would be to focus on utilizing the existing parameters in optimizing the whole of S-parameters. So allowing minimization of the off-diagonal S-parameters in addition to the on-diagonal ones would lead to a more decoupled coil solution while only manipulating the matching parameters. Finally, optimizing for B1+ homogeneity simultaneously to S-parameters would lead to added benefits of the method.

5. Conclusions

The proposed extension to co-simulation method reliably and efficiently introduced arbitrary matching networks into the circuit co-simulation routines and achieved coil tuning for resonance and an optimum condition that resembles fully matched coil. Combined with MARIE, MCCS further accurately produced a full EM simulation of the coils.

We first validated MARIE with new MCCS routine to use it to model simple single-channel coupled with Duke digital human body model. Having successfully validated the MCCS routine, we swept through both tuning and matching network parameters to look for the on-diagonal S-parameters global minimum and optimize the coil. While optimizing for all parameters simultaneously is a viably efficient option for coil models of low complexity, these models are not realistic, and we found that it becomes a highly computationally expensive problem to solve for more complex coil geometries, such as birdcage coils and pTx coils with higher number of channels, especially when shielding is included. Consequently, and to mimic the real-scanner situation, we separated tuning and matching into two steps, by first tuning the coil to the 7T-

equivalent frequency, and then introducing matching networks to enhance the power transmission into the body, and enable better matching. Out of the 4 coils examined (2n, 2s, 8n, 8s), we observed lower on-diagonal S-parameters after matching in all 4, but some, especially the 8n coil, still had strong cross-coupling suggesting high power losses through the adjacent channels, and hence a non-efficient power transfer to the body. Still, the obtained S-parameter values were within the range of values suggested in the literature, so fixing them, the optimization of the coil parameters in tune-and-matching the coil was defined as successful. Finally, we observed successful combination of EM fields obtained with MARIE for every port excited separately, into the fields for every channel excited separately using MCCS. Then for the selected combination of phases to give a circularly polarized mode of operation in coil, we observed that it was indeed possible to efficiently achieve a qualitatively satisfying CP-mode B1+ using MARIE+MCCS.

Even though we successfully introduced matching into the CCS routine and applied it with MARIE in coil tuning-and-matching and field combination for the full EM solution, the method could be far improved, as suggested by the circuit spatial optimization study. Nevertheless, the conditions selected for the coil operation are well within the reported literature values, so we propose further usage of MARIE+MCCS to obtain full-field solutions. This protocol could then be repeated for many different body-coil positional configurations to characterize a large positional safety study at 7T, which is the biggest advantage of using efficient methodologies such as MARIE+MCCS.

Acknowledgments

This work was funded by the King's College London & Imperial College London EPSRC Centre for Doctoral Training in Medical Imaging (EP/L015226/1). This work was supported by the core funding from the Welcome/EPSRC Centre for Medical Engineering [WT203148/Z/16/Z] and by the National Institute for Health Research (NIHR) Biomedical Research Centre based at Guy's and St Thomas' NHS Foundation Trust and King's College London and/or the NIHR Clinical Research Facility. The views expressed are those of the author(s) and not necessarily those of the NHS, the NIHR or the Department of Health and Social Care.

References

[1] Schmidt, R. & Webb, A. *IEEE Trans. Med. Img* **35**, 1837–1844 (2016).
[2] Deniz, C. M. *Topics in Mag. Res. Img.* **28**, 159–171 (2019).
[3] Mao, W., Smith, M. B. & Collins, C. M. *Magn. Reson. Med.* **56**, 918–922 (2006).
[4] Hetherington, H. P., Avdievich, N. I., Kuznetsov, A. M. & Pan, J. W. *Magn. Reson. Med.* **63**, 9–19 (2010).
[5] Oezerdem, C. *et al. Magn. Reson. Med.* 75(6), 2553-2565 (2015).
[6] Guérin, B. *et al. Magn. Reson. Med.* **73**, 1137–1150 (2015).
[7] Adriany, G., Van de Moortele, P.F., Ritter, J., Moeller, S. & Ugurbil, K. *Magn. Reson. Med.* 59(3), 590-597 (2008).
[8] Li, X., Pan, J. W., Avdievich, N. I., Hetherington, H. P. & Rispoli, J. V. *Magn. Reson. Med.* **85**, 3463–3478 (2021).
[9] Li, X. & Rispoli, J. V. *Magn. Reson. Med.* **81**, 1307–1321 (2019).
[10] Kozlov, M. & Turner, R. *J Magn. Reson.* **200**, 147–152 (2009).
[11] Zhang, R., Xing, Y., Nistler, J. & Wang, J. *Proc. ISMRM* (2009).
[12] Lemdiasov, R. A., Obi, A. A. & Ludwig, R. *Concepts Magn. Reson.* **38A**, 133–147 (2011).
[13] Beqiri, A., Hand, J. W., Hajnal, J. V. & Malik, S. J. *Magn. Reson. Med.* **74**, 1423–1434 (2015).
[14] Yang, Q. X. *et al. Magn. Reson. Med.* **47**, 982–989 (2002).
[15] Rivera, D. *et al. NMR Biomed.* **33**, (2020).
[16] Shajan, G. *et al. Magn. Reson. Med.* **71**(2), 870-879 (2014).
[17] Avdievich, N. I., Pan, J. W. & Hetherington, H. P. *NMR Biomed.* **26**, 1547–1554 (2013).
[18] Beqiri, A., Hand, J. W., Hajnal, J. V. & Malik, S. J. *Magn. Reson. Med.* **74**, 1423–1434 (2015).
[19] Villena, J. F. *et al. IEEE Trans. Biomed. Eng.* **63**, 2250–2261 (2016).
[20] Christ, A. *et al. Phys. Med. Biol.* **55**, N23–N38 (2010).

[21] Geuzaine, C. & Remacle, J.-F. *Int. J. Numer. Meth. Eng.* **79**, 1309–1331 (2009).
[22] Ajanovic, A., Tomi-Tricot, R., Hajnal, J.V. & Malik, S. J. *Proc. ICADET,* 1108-1117 (2024).
[23] Ajanovic, A., Hajnal, J. V. & Malik, S. J. *Proc. ISMRM* (2020).
[24] Ajanovic, A., Hajnal, J. V. & Malik, S. J. *Proc. ISMRM* (2021).
[25] Polimeridis, A. G., Reid, M. T. H., Johnson, S. G., White, J. K. & Rodriguez, A. W. *IEEE Trans. Antennas Propagat.* **63**, 611–620 (2015).
[26] Polimeridis, A. G., Villena, J. F., Daniel, L. & White, J. K. *J Comp. Phys.* **269**, 280–296 (2014).
[27] Georgakis, I. P., Giannakopoulos, I. I., Litsarev, M. S. & Polimeridis, A. G. Preprint at arxiv.org/abs/1902.02196 (2020).
[28] Giannakopoulos, I. I. *et al. IEEE Trans. Antennas Propagat.* **70**, 459–471 (2022).
[29] Giannakopoulos, I. I. *et al.* Preprint at arxiv.org/abs/2206.12409 (2022).
[30] Ajanovic, A., Ogier, S., Tomi-Tricot, R., Hajnal, J. V. & Malik, S. J. *Proc. ICADET.* 1138-1148 (2024).
[31] Ajanovic, A., Tomi-Tricot, R., Hajnal, J. V. & Malik, S. J. *Proc. ISMRM* (2023).
[32] Milshteyn, E. *et al. Magn. Reson. Med.* **85**, 429–443 (2021).
[33] Malik, S. J., Hand, J. W., Carmichael, D. W. & Hajnal, J. V. *Magn. Reson. Med.* **88**, 1434–1449 (2022).